Bull. Mater. Sci., Vol. 40, No. 2, April 2017, pp. 307–320. © Indian Academy of Sciences.
DOI 10.1007/s12034-017-1370-8

Mechanical and morphological investigation of virgin polyethylene and silver nanoparticle-loaded nanocomposites film: comprehensive analysis of kinetic models for non-isothermal crystallization

RAJESH KUMAR SAHOO[1,*], BISHNU PRASAD PANDA[1], SANJAY KUMAR NAYAK[1,2] and SMITA MOHANTY[1]

[1]Laboratory for Advanced Research in Polymeric Materials (LARPM), Central Institute of Plastics Engineering and Technology (CIPET), Bhubaneswar 751 024, India

[2]Central Institute of Plastics Engineering and Technology, Chennai 600 032, India

MS received 14 February 2016; accepted 27 June 2016

Abstract. **This research was accomplished to examine the mechanical, morphological and crystallization kinetics study of polyethylene/silver nanoparticles (Ag-NPs) nanocomposite films. In this research, low-density polyethylene (LDPE) nanocomposite films were prepared containing Ag-NPs using maleic-anhydride-grafted low-density polyethylene (LDPE-g-MAH) as a compatibilizer by the melt mixing process. From mechanical property evaluation, it is revealed that the LDPE/LDPE-g-MAH/Ag-NPs nanocomposite films showed decreased tensile strength as compared with virgin LDPE matrix. Thermal characteristics of the prepared virgin LDPE and its nanocomposite films were studied by differential scanning calorimetry (DSC). Comprehensive analysis of different kinetic models such as the Avrami and Mo model on non-isothermal crystallization kinetics was performed in order to correlate the rate of crystallization and its various kinetic parameters. Further, the macrokinetic equation as proposed by Malkin has been applied to describe the kinetics of crystallization in the light of the Avrami equation. Concerning virgin LDPE and Ag-NP-reinforced LDPE, the former shows primary crystallization, whereas the later exhibits both primary and secondary crystallization with varying Avrami exponents. Kinetic parameters are recognized, and confirm the influence of Ag-NPs on crystallization kinetics. X-ray diffraction spectroscopy and transmission electron microscopic analysis of the nanocomposite films were conducted to verify the dispersion of inorganic filler particles in the resulting hybrids.**

Keywords. **Primary crystallization; Ag-NPs; nanocomposites; non-isothermal crystallization; macrokinetic equation.**

1. Introduction

Low-density polyethylene (LDPE) is one of the most widely used commercial polymers in the industrial field, most preferably in food packaging applications because of its magnificent physical and mechanical properties such as acceptable flexibility, thermal stability, environmental recyclability and transparency [1]. The semi-crystalline thermoplastic LDPE also finds broad range applications because of its easy processability, light weight and chemical resistance. The thermal and mechanical properties of the polymer can be considerably enhanced by adding fillers, which act as reinforcing agents. Metal nanoparticles are useful fillers with larger surface area. When these metal nanoparticles are mixed with the thermoplastic polymer, they enhance the crystallization rate of semi-crystallization polymers. Silver nanoparticles (Ag-NPs) are one such metal nanoparticles which have been extensively used to improve the mechanical, thermal and multifunctional properties of the polymer nanocomposites. Further, Ag-NPs are perhaps the metal nanoparticles most used as antimicrobial agents in polymeric nanocomposites in spite of their high cost. Polymer/Ag-NPs nanocomposite films have found enormous use in food industries for packaging as food storage containers, fresh food bags and other cosmetics along with biological, biomedical and pharmaceutical applications. Packaging materials and pharmaceutical apparatus require very high degree of hygienic and purity. The addition of small quantity of Ag-NPs in the preparation of nanocomposite films does not cost much in comparison with its effective bactericidal properties. Further, its potential advantages can be widely used in many consumer products without due contemplation of the cost–benefit ratio. Ag-NPs can also be used as antiviral and antifungal agents. Quite a few methods have also been adopted to synthesize LDPE/Ag-NPs nanocomposite films, including *in-situ* polymerization, solvent blending and melt compounding [2]. LDPE/Ag-NPs nanocomposites with low release potential of silver ion showed excellent long-term antimicrobial activity. It has been confirmed that the prolonged and steady release of Ag^+ ions is enhanced and hence the antimicrobial properties are enhanced in the aqueous atmosphere.

*Author for correspondence (rajeshshreeparnasahoo@gmail.com)

As the polymer crystallinity affects the release of Ag^+ ions, the study of crystallization kinetics is of prime importance.

The overall properties of thermoplastic polymers depend principally on the degree of crystallinity, crystalline structure and morphology [3,4]. In any heat transfer issues the progress of crystallization and magnitude of the spherulites formation necessarily depend upon the enthalpy of conduction and hence they are coupled with energy equations. Therefore, it is essential to find a differential form of the kinetic equations that could merge into the differential heat transfer expressions, which is important to understand the different kinetic variables controlling the process of crystallization [5]. There are two different types of thermal conditions usually used to study the kinetics of crystallization. One is isothermal crystallization and another is non-isothermal crystallization [6]. During the study of crystallization kinetics under isothermal condition, the problems related to cooling rates and thermal gradients are overlooked [7,8], but under the non-isothermal condition the measurements of kinetic parameters are very much required. These kinetic parameters are quite helpful in resolving the issues relating to processing and property measurements [9]. Similarly, within a limited time period, large quantity of information can be obtained using the non-isothermal crystallization method. The difficulty resides in optimization of the process parameters like mould temperature, the temperature of the melt and cooling conditions to minimize the residual stresses. To do this, it is pertinent to calculate the temperature and its alteration patterns in the path of crystallization. In addition, semi-crystalline polymers normally crystallize between their melting temperature and their glass-transition temperature. Depending upon the initiation stage from which polymer chains are brought to crystallize, bulk crystallization can be classified into two types. They are melt crystallization and cold crystallization. The former is the case where the polymers are brought to crystallize from a temperature higher than melting temperature [6]. On the contrary, if the polymers are brought to crystallize from the glassy state, i.e., temperature lower than glass-transition temperature, it is known as cold crystallization. Both physical and mechanical properties of semi-crystalline polymers strongly depend on the rate of crystallization, the extent of crystallite formation and the morphological changes that occur during processing time. Therefore, it is pertinent to mention that studies related to crystallization kinetics provide valuable information for gaining a thoughtful relationship among the processing conditions and the properties of the finished products [7].

In order to illustrate the crystallinity under non-isothermal conditions, a number of macroscopic mathematical models have been constructed. From literature review, the wide use of Avrami [8–10], Ozawa [11], Tobin [12–14] and the Malkin [15,16] models relating to crystallization behaviour of polymers was seen. The Avrami equation, which is extensively used in many research papers, is based on a simple mathematical equation possessing the basic theoretical concept and the full explanation of the investigational data in existent polymeric systems [17]. The use of the Malkin equation to analyse the non-isothermal crystallization data of semi-crystalline polymer and its nanocomposites is uncommon and is based on various mathematical models that are different from the Avrami macrokinetic model. A qualitative comparison between the Avrami and the Malkin models was carried out based on the isothermal crystallization data of polyethylene (PE), isotactic polypropylene (i-PP), PET and polyurethane (PU) [18]. The experiments carried out to verify the adequacy of such kinetic models have shown a mismatch between calculated values and the experimentally determined ones. The differences may result from the uncertainty of the non-isothermal crystallization mechanisms derived from the Avrami equation [19–21]. It should also be emphasized that the Avrami equation is not convenient for use in a non-isothermal situation, but its differential form is considered jointly with the heat transfer equation to solve the complex crystallization mechanism [22]. Besides, the Avrami equation applies merely to single-stage crystallization (primary crystallization) and is not adequate during the secondary stage of the crystallization process. Mo and co-workers have also published many research papers on the non-isothermal crystallization process of polymers [23]. They derived an equation for describing the non-isothermal crystallization kinetics of polymer obtained by combining the Avrami equation and Ozawa equation [19]. This research paper will study different kinetic equations, which will give the solution to various process-related problems and also fit well to the experimental data.

In the present investigation, LDPE/Ag-NPs nanocomposite films have been prepared by melt blending technique using virgin LDPE polymer and Ag-NPs as filler along with maleic-anhydride-grafted polyethylene (LDPE-g-MAH) as compatibilizer. The synergetic effect on mechanical and thermal properties has been comprehensively studied. X-ray diffraction (XRD) and transmission electron microscopy (TEM) studies have been performed to know the mixing characteristic of Ag-NPs inside the polymer matrix and morphological characteristic of the nanocomposites.

2. Theoretical background

Studies related to the overall kinetics of non-isothermal crystallization of semi-crystalline polymers and their nanocomposites in DSC analysis are based on the information obtained from the crystallization exotherms. As the rate of crystallization depends on the surface area of the crystallites, greater the surface area of the crystallites, more is the rate of crystallization. Based on this postulation, the relative crystallinity (X_t) as a function of time can be obtained by integrating the crystallization exotherms according to the differential equation

$$X_t = \frac{\int_0^t (\mathrm{d}H_c/\mathrm{d}t)\,\mathrm{d}t}{\Delta H_c}, \tag{1}$$

where t is the elapsed time and $\mathrm{d}H_c$ the enthalpy of crystallization in an infinitesimal time interval $\mathrm{d}t$. ΔH_c is the

total enthalpy of crystallization at a particular crystallization temperature, which is defined as

$$\Delta H_c = \int_0^\infty \left(\frac{dH_c}{dt}\right) dt \tag{2}$$

The Avrami equation could be derived from the modified first-order kinetic model [24], which reads as

$$dX_t/dt = SK'(1 - X_t), \tag{3}$$

where S represents the surface area of the crystallites above which the macromolecular segments can be deposited. K' is a constant at a particular temperature. Considering the assumption that the numbers of nuclei formed during the process of crystallization simultaneously grow in three dimensions into spherulites, it is possible to relate the total surface area of the crystallites with the radius of a spherulite (r) as

$$S = 4\pi N_0 r^2, \tag{4}$$

where N is the number of nuclei per unit mass and volume of the spherulites can be can be expressed as

$$V = (4/3)\pi N_0 r^3 \tag{5}$$

Putting the value of r in eq. (4), the expression for surface area is

$$S = 4\pi N_0 \frac{3V}{(4\pi N_0)^{2/3}}. \tag{6}$$

From eqs (1) and (2) the Avrami equation governing the phase transformation is expressed as [25]

$$X_t = 1 - \exp[-(K_a t)^{n_a}], \tag{7}$$

where K_a is the Avrami rate constant and n_a is the Avrami exponent. Both the constants are distinctive for particular crystallization condition and crystallization morphology. K_a is specific to a given crystalline morphology and n_a is related to the type of nucleation and growth mechanisms. The value of the Avrami exponent n_a should be fractional [9,26,27].

2.1 *Macrokinetic equation*

The macrokinetic description of the crystallization process of virgin polymer and its nanocomposite is represented as [28,29]

$$\acute{\eta} = \acute{\eta}(T, \eta), \tag{8}$$

where $\acute{\eta}$ is the crystallization rate and η is the degree of crystallinity.

Primary crystallization is supposed to cease when no more molecular chains enter into the growth surface. This may be because of the impregnation of crystalline aggregates. On the other hand, the secondary crystallization may refer to further extension of the crystallization process, which means the increase in crystallinity after the cessation of primary crystallization. Therefore combining both the stages of nucleation and growth, eq. (8) can be written as

$$\acute{\eta}(T, \eta) = \acute{\eta}_1(T, \eta) + \acute{\eta}_2(T, \eta), \tag{9}$$

where $\acute{\eta}_1$ is the rate at which the degree of crystallinity varies as a result of the emergence of the primary nuclei and $\acute{\eta}_2$ is the rate of variation in the degree of crystallinity due to spherulitic growth or interlamellar crystallization.

Further, $\acute{\eta}_1$ is related as

$$\acute{\eta}_1 = I W_0, \tag{10}$$

where I is the ongoing rate of nucleation and W_0 is the critical volume of an equilibrium nucleus.

The crystal growth rate $\acute{\eta}_2$ is related as

$$\acute{\eta}_2 = G_0 S / V_0, \tag{11}$$

where G_0 is the linear growth rate and V_0 is the total volume of the sample.

Thus

$$\acute{\eta} = I W_0 + G_0 S / V_0. \tag{12}$$

The current rate of nucleation (I) is written as [30]

$$I = I_0(1 - X_t), \tag{13}$$

where I_0 is the nucleation rate and X_t is the degree of crystallinity. The total surface area $S(X_t)$ over which the crystallization takes place is basically the product of free growth function $\dot{S}(X_t)$ and $(1 - X_t)$ [27]. Hence $S(X_t)$ is expressed as follows:

$$S(X_t) = \dot{S}(X_t)(1 - X_t). \tag{14}$$

Further, the degree of crystallinity can be expressed as $X_t = q(t)/Q_{cry}$, where $q(t)$ is heat content during the crystallization process and is related as $q(t) = \Delta H \eta$, and Q_{cry} is the heat of crystallization, which is related as $Q_{cry} = \Delta H \eta^0_{eq}$ and

$$X_t = \eta/\eta^0_{eq}, \tag{15}$$

where η^0_{eq} is the equilibrium degree of crystallinity.

Thus

$$1 - X_t = 1 - (\eta/\eta^0_{eq}) = (\eta^0_{eq} - \eta)/\eta^0_{eq}.$$

Hence eq. (13) can be written as follows:

$$I = I_0[(\eta^0_{eq} - \eta)/\eta^0_{eq}]. \tag{16}$$

Similarly eq. (14) can be written as follows:

$$S(X_t) = \dot{S}(\eta)(\eta^0_{eq} - \eta)/\eta^0_{eq}. \tag{17}$$

Hence, eq. (12) can be written as follows:

$$\frac{d\eta}{dt} = \acute{\eta} = K_0(\eta^0_{eq} - \eta)(1 + A_0\dot{S}(\eta)), \tag{18}$$

where $K_0 = I_0 W_0/\eta^0_{eq}$ and $A_0 = G_0(V_0 I_0 W_0)^{-1}$.

Thus, eq. (18) derived using macrokinetic approaches is a depiction of both isothermal and non-isothermal cases. The macrokinetic equation for crystallization can be stated as follows:

$$\dot{X}_t = [A_1 + A_2\dot{S}(X_t)](1 - X_t), \tag{19}$$

where $\dot{X}_t$ is the crystallization rate, $A_1 = K_0$ corresponds to the initial rate and $A_2 = K_0 A_0$ corresponds to the auto-acceleration effect.

2.2 *Comparison of the macrokinetic and Avrami equation*

Comparing eq. (3) with eq. (19), it is seen that eq. (3) is a particular case of eq. (19). The differential form of eq. (3) is

$$\frac{1}{1-X_t} = K^{1/n}(n)\left(\ln\frac{1}{1-X_t}\right)^{(n-1)/n}. \tag{20}$$

Similarly eq. (15) can be expressed as follows:

$$\frac{1}{1-X_t}\frac{\mathrm{d}X_t}{\mathrm{d}t} = A_1 + A_2\dot{\mathrm{S}}(X_t). \tag{21}$$

Considering the variation in the degree of crystallinity with the crystal growth rate, Malkin *et al* [15] arrived at a totally new equation considering the relation between eqs (3) and (15), which is written as follows:

$$X_t = \frac{C_{0+1}}{C_{0+e}C_{1t}}, \tag{22}$$

or

$$e^{-kt^n} = \frac{C_{0+1}}{C_{0+e}C_{1t}}, \tag{23}$$

where C is the Malkin exponent. It is related directly to the ratio of the linear crystal growth rate G to the primary nucleation rate I. It is expressed as $C_0 = A_2 G/I$, where A_2 is a specific rate constant.

C_1 is the Malkin crystallization rate constant, which relates directly to the overall crystallization rate. It is expressed as $C_1 = A_2 G + I$. The dimension of C_1 is $(\text{time})^{-1}$.

3. Experimental

3.1 *Materials*

Film-grade LDPE, 1005FY20, produced by a high-pressure autoclave process was obtained from Reliance Industries Ltd., India, with MFI of 0.5 g/10 min at the rate of 230°C/2.16 kg having the density of 0.92 g cm^{-3}. LDPE-g-MAH has been purchased from M/S Pluss Polymers, Haryana, India. Its density is 0.908 g cm^{-3} and MFI is 110 g/10 min at the rate of 230°C/2.16 kg. The commercial grade Ag-NPs used in this experiment is of 99.9% purity having average particle size ranging from 50 to 80 nm with specific surface area of 5.37 m^2 g^{-1}. It is in fine powder form with bulk density of 0.312 g cm^{-3} and true density of 10.5 g cm^{-3} obtained from Nanoshel, Intelligent Materials Pvt. Ltd., Panchkula, Haryana, India.

3.2 *Sample preparation*

The LDPE/Ag-NPs nanocomposite films were prepared by the melt compounding technique. The nanocomposite films were obtained using a torque rheometer (Haake Rheomix OS, Germany) with counter-rotating roller rotors. The screw speed was maintained at 100 rpm. The time period of 15 min as holding time was set for homogeneous dispersion of all the materials used for the preparation of nanocomposites. The barrel temperature at feeder zone is maintained at 175°C and at the die zone the temperature is maintained at 190°C. Before extrusion, the Ag-NPs powder was dried in a vacuum chamber at 80°C for 24 h to get rid of the moisture. The composition of each master batch containing Ag-NPs was in the range of 0.5, 1.5 and 2.5% by weight. After melt mixing, the compounded material was extruded in cylindrical forms. The cylindrical extrudes were pelletized and processed to produce the desired films of thickness ~0.01 mm. After evaluating the mechanical properties of the nanocomposite films, the optimized sample was further compounded with different weight percentages (3, 5 and 7 wt%) of the compatibilizer. Tensile testing was performed for the prepared compatibilized nanocomposite films. The sample showing optimum mechanical properties has been used for various characterizations and property evaluations.

4. Instruments and conditions

4.1 *Mechanical properties*

Tensile properties were evaluated using a Universal Testing Machine (3882 Instron, UK) according to the ASTM standard. Test specimens were moulded in a size of 3.18 mm (width), 63.66 mm (length) and 3.00 mm (thickness) with a gauge length of 12.5 mm. The tensile strength, tensile modulus and elongation at break for the prepared samples were evaluated at a crosshead speed of 50 mm min^{-1}.

4.2 *Differential scanning calorimetry (DSC) analysis and analytical procedures*

A differential scanning calorimeter (Q20, TA Instruments, USA) was equipped with the internal cooling unit, which provides a cooling rate up to 200°C min^{-1}. Each sample holder was loaded with a single disc pan weighing 5–8 mg of sample cut from the prepared film in order to minimize the thermal lag between the sample and DSC sensors. Each sample was used only once at a time and all experiments were run under nitrogen atmosphere. For non-isothermal crystallization kinetic study the samples were cooled at various cooling rates of 5, 10, 15 and 20°C min^{-1}. Initially, the sample was heated starting from the negative temperature of 50°C. Then the sample was heated to a temperature of 200°C at a scanning rate of 80°C, where it was held for 5 min, to ensure complete mixing and erase the previous thermal history [18]. The result obtained from DSC analysis was the input to a multi-variable regression program to fit the experimentally computed data into the desired macrokinetic equations.

4.3 *Morphological observation*

Wide-angle XRD (WXRD) analysis was carried out to characterize the mixing of Ag-NPs in the LDPE matrix, using a

Shimadzu MAXima_XRD-7000 X-ray diffractometer with a filtered Cu-Kα radiation source ($\lambda = 1.54$ Å) at the operating voltage 40 kV and current of 30 mA with a 2D detector. The XRD patterns of Ag-NPs as well as the melt-blended LDPE/LDPE-g-MAH/Ag-NPs nanocomposites were examined over a range of diffraction angle 2θ from 35° to 80° with scanning rate and step size of 0.5° min^{-1} and 0.02°, respectively. The morphology of the LDPE/LDPE-g-MAH/Ag-NPs nanocomposite films was also observed using a transmission electron microscope (JEOL 1200EX, Japan). An ultra-thin sample of 80-nm thickness was microtomed under cryogenic conditions, using a Leica EM UC7 ultra-microtome equipped with a diamond knife (M/s Leica, Germany) for subsequent TEM observations. Images were captured by means of a charged couple detector (CCD) camera for investigation with the help of a software called Granton Digital Micrograph.

5. Results and discussion

5.1 *Mechanical property study*

The mechanical properties of virgin LDPE and its nanocomposite films are presented in table 1. It is evident that the addition of Ag-NPs into the LDPE matrix results in a decrease in the tensile strength of LDPE. The tensile properties largely depend on the composition of the nanocomposite, chemical structure of the matrix and level of dispersion of the filler within the matrix. Loading of 0.5 wt% of Ag-NPs decreases the tensile strength of the nanocomposite film by 20.77%, and for loading of 1.5 wt% of Ag-NPs the decrease in tensile strength of the nanocomposite film is 20.68% as compared with the virgin LDPE film. Further loading of Ag-NPs significantly reduces the tensile strength of the LDPE/Ag-NPs nanocomposite film. Azlin-Hasim *et al* [31] have also reported a similar decrease in tensile strength and modulus on the addition of Ag-NPs (more than 0.3 wt%) to virgin LDPE. This behaviour might be due to the reduction in stretching potential and discontinuity of the polymer network structure [32]. Further, the hydrophilic nature of Ag-NPs and the hydrophobic nature of LDPE polymers are incompatible for mixing. Therefore the interfacial attraction between them is poor, which resulted in the decrease in strength of the nanocomposite film.

From table 1, it is seen that there is a minor decrease in tensile modulus on the addition of 0.5 wt% Ag-NPs to virgin LDPE matrix. The addition of 1.5 wt% of Ag-NPs to PE matrix shows marginal (∼2.95%) increase in modulus. The overall observation is that the modulus of the nanocomposite film did not change significantly and it is independent of Ag-NPs concentration as compared to the virgin LDPE film. This is due to the formation of Ag-NPs agglomerates inside the nanocomposite film. Hanemann and Szabó [33] reported that there is no enhancement of tensile modulus in thermoplastic polymeric materials when nano-sized particles formed aggregates inside the nanocomposite network structure. Further, nanocomposite films exhibit drastic reduction in the percentage of elongation at break at different Ag-NPs loadings. This is due to imperfect polymer–filler interaction at the interlocking point in the nanocomposite structure.

The effect of the addition of compatibilizer of variable concentration to of Ag-NP-loaded LDPE nanocomposite film with a fixed concentration (1.5 wt%) of Ag-NPs was studied. It was found that the addition of compatibilizer did not show any improvement in tensile strength of nanocomposite film as compared to the virgin LDPE film, but marginal enhancement was shown in tensile modulus (∼3.21%) on the addition of 3 wt% LDPE-g-MAH. Hence, the presence of compatibilizer shows little effect on mechanical properties of the nanocomposite film. This indicates that LDPE-g-MAH does not help much in miscibility of Ag-NPs within LDPE matrix. Therefore, nanocomposite films have the minimum effect on mechanical properties as compared to virgin LDPE film.

5.2 *Thermal characteristics*

5.2a *Crystallization study*: The crystallization endotherms of LDPE and LDPE/LDPE-g-MAH/Ag-NPs (95.5:3:1.5) nanocomposite film at different cooling rates are presented, respectively, in figures 1 and 2. There is an overall increase in thermal stability of the LDPE matrix on the addition of Ag-NPs. Similar findings have also been reported for thermoplastic polypropylene/Ag-NPs nanocomposites [34]. The positive shift in thermal stability is because of the presence of Ag-NPs in the matrix, which suppress the motion of the polymer molecular chains and their interlocking points.

Table 1. Mechanical properties of LDPE and its nanocomposite films.

Sample/composition	Tensile strength (MPa)	Elongation at break (%)	Tensile modulus (MPa)
Virgin LDPE	11.94	501.67	81.51
LDPE/0.5 wt% Ag-NPs	9.46	188.14	80.52
LDPE/1.5 wt% Ag-NPs	9.47	175.58	83.92
LDPE/2.5 wt% Ag-NPs	8.71	173.80	79.13
LDPE/LDPE-g-MAH/Ag-NPs (95.5:3:1.5)	9.98	178.89	84.13
LDPE/LDPE-g-MAH/Ag-NPs (93.5:5:1.5)	9.64	175.51	83.45
LDPE/LDPE-g-MAH/Ag-NPs (91.5:7:1.5)	9.37	173.56	83.78

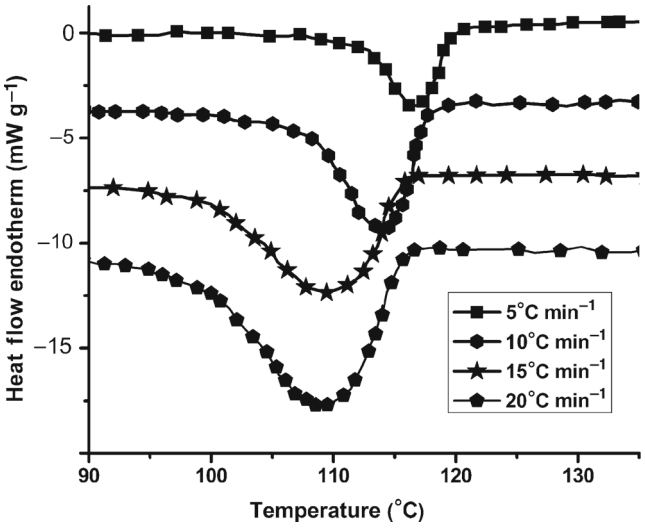

Figure 1. Crystallization thermograms of virgin LDPE film recorded during non-isothermal crystallization at different cooling rates in a definite temperature range.

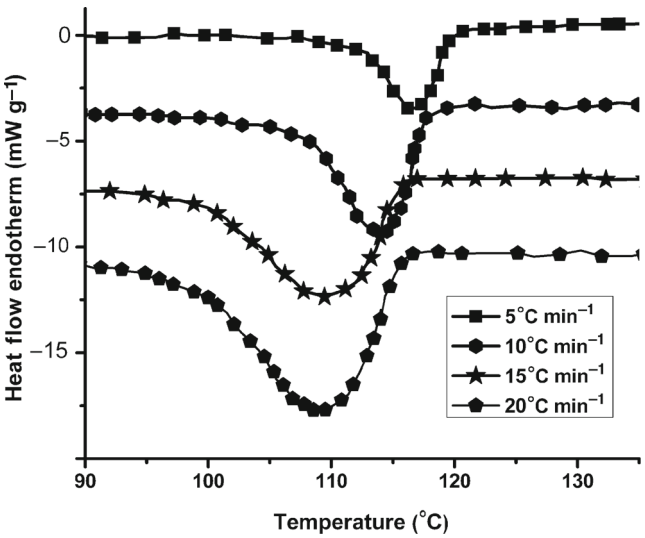

Figure 2. Crystallization isotherms of LDPE/LDPE-g-MAH/Ag-NPs (95.5:3:1.5) nanocomposite film recorded during non-isothermal crystallization at different cooling rates.

From the curves, some important parameters, like the temperature attained at 1% relative crystallinity ($T_{0.01}$, called T_c), the crystallization peak temperature (T_p), the temperature attained at 99% relative crystallinity ($T_{0.99}$) and crystallization temperature range (ΔT_c) were determined and are listed in table 2. It is seen that the peaks of the endothermic graphs shift to lower temperature as the cooling rate increases. T_p shifts to lower value and the peak becomes broader for virgin LDPE and LDPE/LDPE-g-MAH/Ag-NPs (95.5:3:1.5) nanocomposite film. The value of T_p decreases from 114.27 to 107.24°C for virgin LDPE and 116.23 to 107.45°C for LDPE/LDPE-g-MAH/Ag-NPs (95.5:3:1.5) nanocomposite film for the cooling rate from 5 to 20°C min^{-1}, respectively. This indicates that the degree of super-cooling required for the crystallization reduces when the Ag-NPs are incorporated within the LDPE matrix.

Figure 3 depicts the relationship between T_p and the cooling rate for virgin LDPE and LDPE/LDPE-g-MAH/Ag-NPs (95.5:3:1.5) nanocomposite film. It is seen that as the cooling rate (λ) increases, T_p decreases. For example, T_p of virgin LDPE decreases by about 7°C when cooling rate increases from 5 to 20°C min^{-1} and for LDPE/LDPE-g-MAH/Ag-NPs (95.5:3:1.5) nanocomposite film, T_p decreases by about 9°C. Shifting of T_p to lower temperature indicates the requirement of higher under-cooling to initiate crystallization. Further, the presence of Ag-NPs in LDPE leads to increase in T_p of the nanocomposite film. At the cooling rate of 5°C min^{-1}, T_p for virgin LDPE is ~114°C, while for LDPE/LDPE-g-MAH/Ag-NPs (95.5:3:1.5) nanocomposite film T_p is ~116°C. It implies that the Ag-NPs within the LDPE matrix created smaller spherulites in a heterogeneous nucleation process and act as a nucleating agent for the LDPE matrix. Therefore they accelerate the nucleation rate of the polymer. Similar results have been reported in the literature for Nylon-6/Ag-NPs nanocomposites [35].

Figures 4 and 5 show the relationship between X_t and T_c for LDPE and its nanocomposite film at different cooling rates. The inverse sigmoid shape of the plots signifies that a shifting of relative degree of crystallinity was observed, which is related to the delay effect of the cooling rate on crystallization [36].

Figures 6 and 7 present the plots of relative crystallinity as a function of time. The crystallization time at an arbitrary

Table 2. Summary of kinetic parameters for virgin LDPE and the nanocomposite film.

Sample	Cooling rate λ (°C min^{-1})	T_c (°C)			$\Delta T_c = T_{0.01} - T_{0.99}$ (°C)	$t_{1/2}$ (min)
		$T_{0.01}$	T_p	$T_{0.99}$		
Virgin LDPE	5	117.73	114.27	106.67	11.06	1.20
	10	117.68	113.02	101.92	15.76	1.16
	15	114.32	108.05	95.12	19.2	0.98
	20	112.67	107.24	91.64	21.03	0.84
LDPE/LDPE-g-MAH/ Ag-NPs (95.5:3:1.5)	5	119.78	116.23	110.56	9.22	0.857
	10	117.98	113.19	104.23	13.75	0.449
	15	114.84	108.45	97.86	16.98	0.397
	20	114.67	107.45	92.67	22.0	0.388

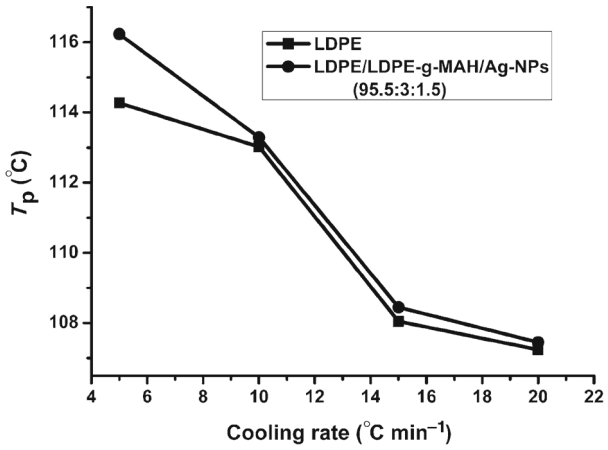

Figure 3. Relationship between crystallization peak temperature (T_p) and the cooling rate for virgin LDPE and LDPE/LDPE-g-MAH/Ag-NPs (95.5:3:1.5) nanocomposite film.

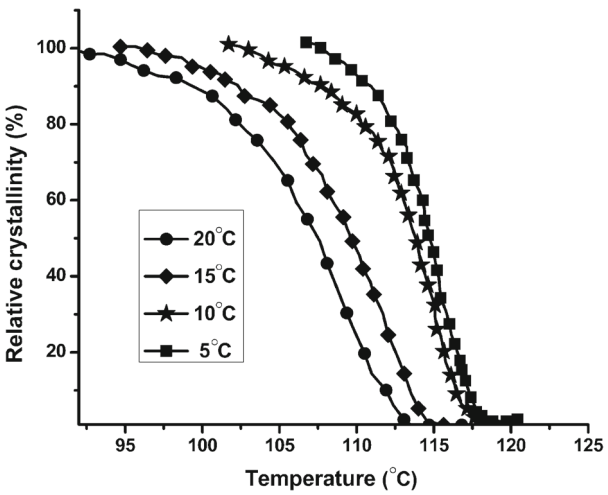

Figure 4. Relative crystallinity (X_t) as a function of crystallization temperature of virgin LDPE.

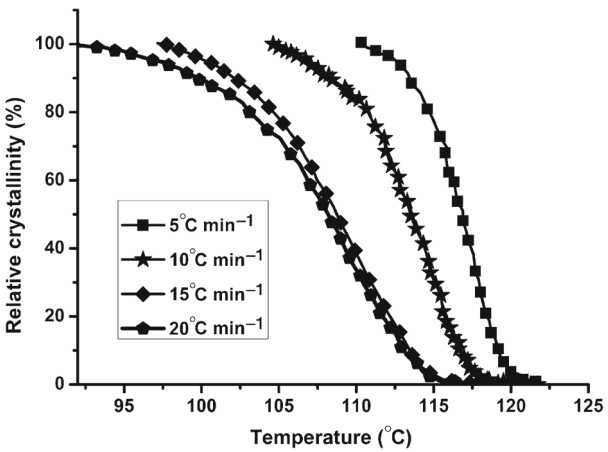

Figure 5. Relative crystallinity (X_t) as a function of crystallization temperature of the LDPE/LDPE-g-MAH/Ag-NPs (95.5:3:1.5) nanocomposite film.

relative crystallinity (t_x) has been determined from the plots and listed in table 3.

The values of crystallization time (t_x) for various relative crystallinity values (i.e., $x = 0.01, 0.1, 0.3, 0.5, 0.9$ and 0.99) for virgin LDPE and LDPE/PE-g-MAH/Ag-NPs (95.5:3:1.5) nanocomposite film have also been listed in table 3. The values of t_x are plotted against λ for LDPE film and LDPE/LDPE-g-MAH/Ag-NPs (95.5:3:1.5) nanocomposite film and presented, respectively, in figures 8 and 9. The crystallization period (ΔT_c) has been calculated and listed in table 3. It is observed that the value of t_x for a given value of x and ΔT_c decreases with the increase in the cooling rate. This suggests faster rate of crystallization. Also, the values of t_x and ΔT_c for LDPE/LDPE-g-MAH/Ag-NPs (95.5:3:1.5) nanocomposite film are lower as compared with LDPE film, which indicates that the Ag-NPs act as a

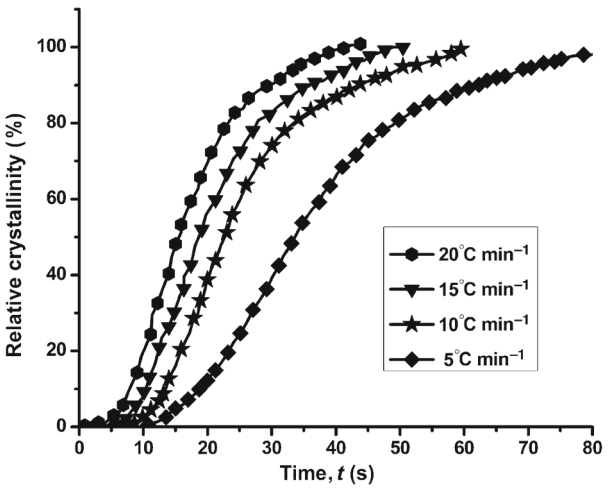

Figure 6. Variation of relative crystallinity (X_t) as a function of time of virgin LDPE.

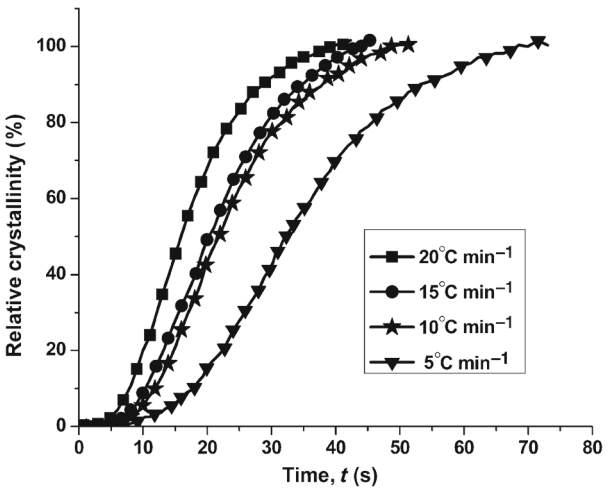

Figure 7. Variation of relative crystallinity (X_t) as a function of time of LDPE/LDPE-g-MAH/Ag-NPs (95.5:3:1.5) nanocomposite film.

Table 3. Summary of crystallization time at various relative crystallinity values (t_x) of virgin LDPE and its nanocomposite film at different cooling rates.

		t_x (min)						
Sample	λ (°C min^{-1})	$x = 0.01$	0.1	0.3	0.5	0.9	0.99	ΔT_c
Virgin LDPE	5	0.16	0.31	0.44	0.56	1.03	1.33	1.17
	10	0.12	0.21	0.29	0.37	0.72	0.96	0.84
	15	0.11	0.17	0.24	0.30	0.59	0.80	0.69
	20	0.07	0.11	0.18	0.25	0.49	0.66	0.59
LDPE/LDPE-g-MAH/ Ag-NPs (95.5:3:1.5)	5	0.12	0.29	0.42	0.54	0.91	1.05	0.93
	10	0.10	0.18	0.28	0.35	0.63	0.80	0.71
	15	0.07	0.17	0.24	0.32	0.56	0.71	0.64
	20	0.05	0.11	0.17	0.25	0.47	0.64	0.59

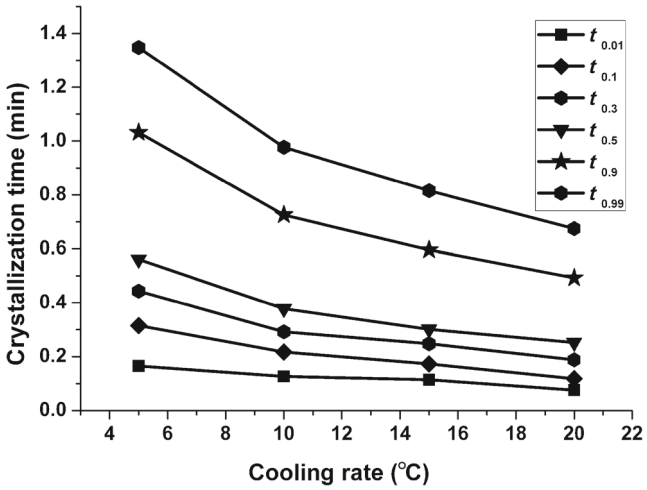

Figure 8. Crystallization time at various relative crystallinity values as a function of cooling rate of virgin LDPE film.

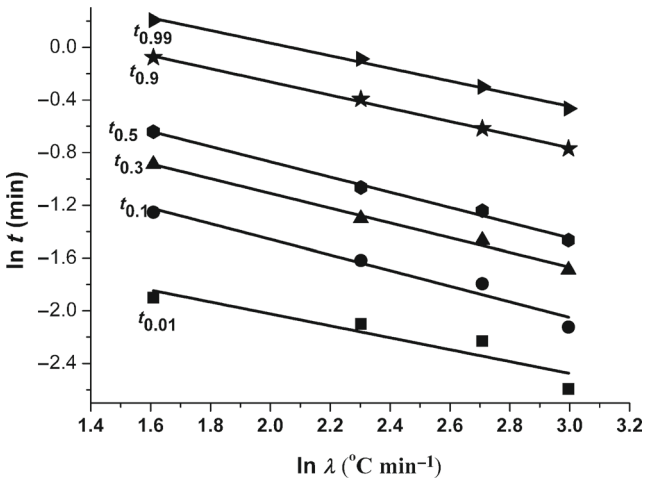

Figure 10. Crystallization time at various relative crystallinity values as a function of cooling rate for virgin LDPE.

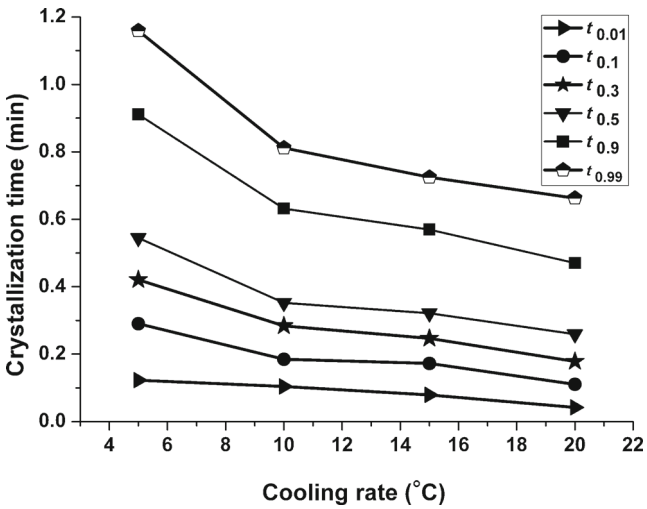

Figure 9. Crystallization time at various relative crystallinity values as a function of cooling rate for LDPE/LDPE-g-MAH/Ag-NPs (95.5:3:1.5) nanocomposite film.

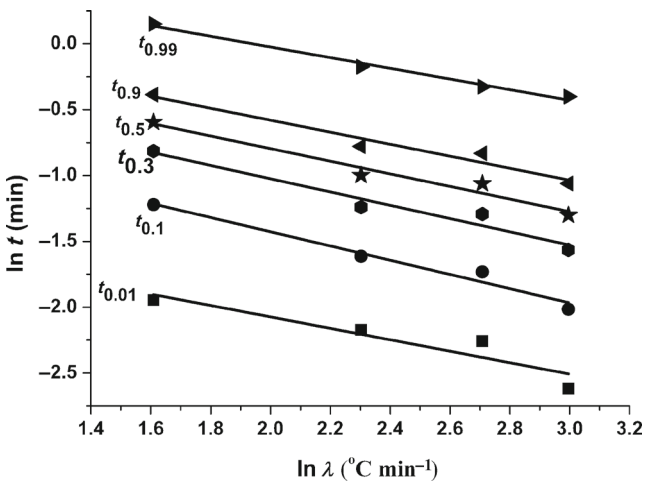

Figure 11. Crystallization time at various relative crystallinity values as a function of cooling rate for LDPE/LDPE-g-MAH/Ag-NPs (95.5:3:1.5) nanocomposite film.

nucleating agent for LDPE matrix and enhance the overall crystallization rate.

In order to infer the computed results, graphs have been drawn between $\ln(t_x)$ and $\ln\lambda$ for the virgin LDPE and LDPE/LDPE-g-MAH/Ag-NPs (95.5:3:1.5) nanocomposite film and shown, respectively, in figures 10 and 11. The linearity of these plots is evident from the graph. From these straight line graphs, y-intercepts, slopes and r^2 have been calculated and listed in table 4. It is seen that y-intercepts of the plots increase with increasing x values. The slopes of all the lines are nearly the same. Similar findings have been reported in the literature for medium-density PE nanocomposite film [37,38]. It confirms the fact that crystallization time is related to the relative degree of crystallinity, which is further related to polymer–filler interaction.

5.2b *Non-isothermal crystallization kinetics based on kinetic models*: In order to analyse the non-isothermal crystallization process, the analysis of the experimental data was carried out using different macrokinetic models.

5.2b1 *Avrami kinetic model*: The double logarithmic form of eq. (7) is written as

$$\ln[-\ln(1 - X_t)] = \ln K_a + n_a \ln(t). \quad (24)$$

Figures 12 and 13 show plot between $[\ln(\ln(1 - X_t))]$ and $\ln(t)$ for virgin LDPE and LDPE/LDPE-g-MAH/Ag-NPs (95.5:3:1.5) nanocomposite film, respectively, at different cooling rates. The Avrami exponent n_a and crystallization rate constant K_a are calculated from the slope and intercept by the linear fit method and summarized in table 5. The Avrami equation does not describe the entire crystallization process and is valid only to the primary stage of the crystallization process. The curved lines display non-linear relationship for most of the portion, indicating fractional value of the exponent n_a. The Avrami exponent n_a is in the range of 3.99–4.87 for virgin LDPE and 3.35–4.67 for LDPE/LDPE-g-MAH/Ag-NPs (95.5:3:1.5) nanocomposite film. The fractional values of Avrami exponent n_a can be understood from the average contribution of occurrence of various modes of nucleation process and growth of the crystallites [39,40]. It is also seen that with increasing cooling rate, there is a steady decrease in the value of Avrami exponent. The higher the value K_a, greater is the crystallization rate. At the same cooling rate, the K_a for nanocomposite film is higher as compared with virgin LDPE film, which indicates that the addition of Ag-NPs into LDPE matrix results in on-time crystallization effectively.

Table 4. Summary of y-intercept, slope and r^2 values of straight lines drawn through plots of $\ln t_x$ against $\ln\lambda$ for various relative crystallinity values.

Sample	x	Intercept	Slope	r^2
Virgin LDPE	0.01	−0.802	−0.452	0.8929
	0.10	−0.140	−0.592	0.9488
	0.30	0.399	−0.559	0.9972
	0.50	0.688	−0.577	0.9900
	0.90	1.087	−0.500	0.9970
	0.99	1.327	−0.480	0.9931
LDPE/LDPE-g-MAH/ Ag-NPs (95.5:3:1.5)	0.01	−1.205	−0.434	0.8944
	0.10	−0.346	−0.540	0.9577
	0.30	−0.016	−0.504	0.9298
	0.50	0.161	−0.478	0.9430
	0.90	0.331	−0.453	0.9380
	0.99	0.786	−0.405	0.9830

5.2b2 *Malkin macrokinetic model*: Figure 14 presents the confirmation of investigational data with respect to the

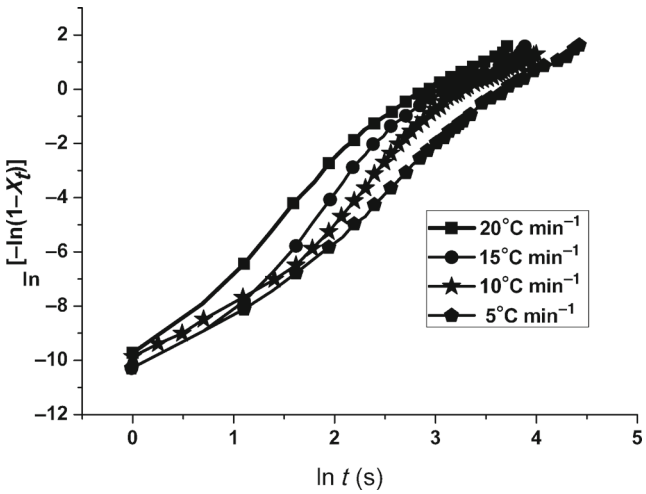

Figure 12. Plots of $[\ln(-\ln(1 - X_t))]$ *vs.* $\ln(t)$ for crystallization of virgin LDPE at different cooling rates.

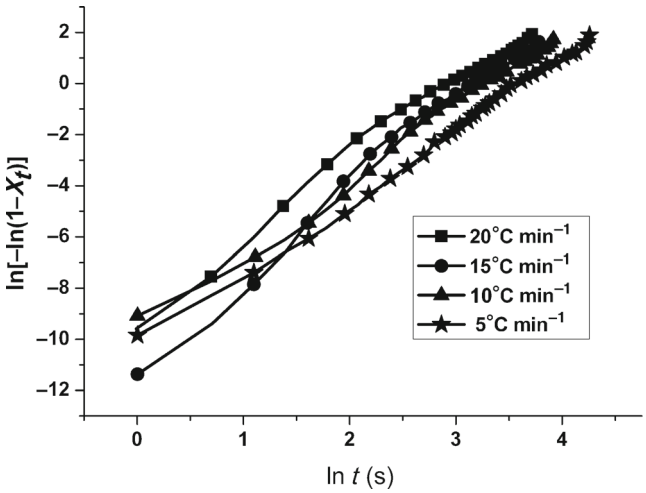

Figure 13. Plots of $[\ln(-\ln(1 - X_t))]$ *vs.* $\ln(t)$ for crystallization of LDPE/LDPE-g-MAH/Ag-NPs (95.5:3:1.5) nanocomposite at different cooling rates.

Table 5. Avrami kinetic parameters (K_a and n_a) for LDPE and LDPE/LDPE-g-MAH/Ag-NPs (95.5:3:1.5) nanocomposite film at different cooling rates.

Sample	λ (°C min^{-1})	n_a	$-\ln K_t$	K_a	r^2
Virgin LDPE	5	4.53	11.0438	0.112	0.98906
	10	4.38	8.98912	0.403	0.96995
	15	4.37	10.19278	0.506	0.96649
	20	3.99	10.53862	0.590	0.98019
LDPE/LDPE-g-MAH/ Ag-NPs (95.5:3:1.5)	5	4.87	8.68929	0.175	0.98078
	10	4.67	10.86664	0.337	0.98009
	15	4.40	9.64913	0.526	0.99144
	20	3.35	10.42664	0.593	0.99559

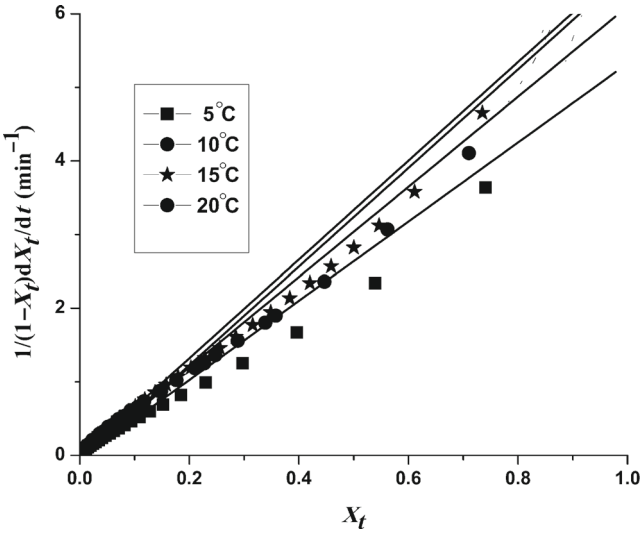

Figure 14. Crystallization isotherm of LDPE: (1) 50, (2) 100, (3) 150 and (4) 200°C min^{-1} cooling rates in coordinates $[1/(1-X_t)](\mathrm{d}X_t/\mathrm{d}t)$ *vs.* X_t; solid line represents the result calculated by using the macrokinetic Malkin equation and symbols indicate the results calculated by using the Avrami equation.

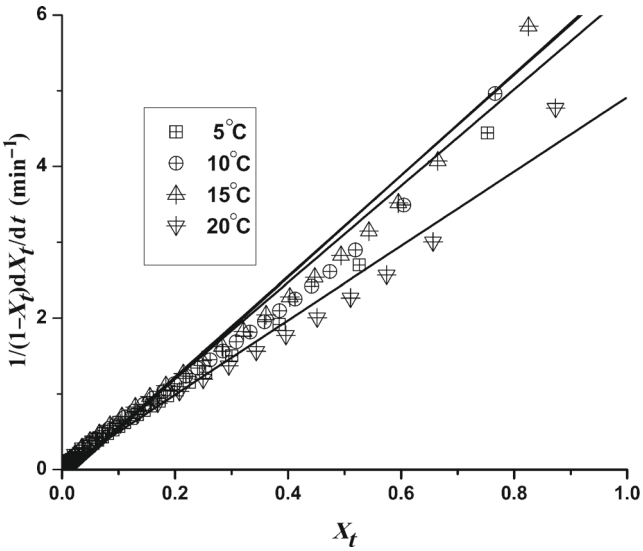

Figure 15. Crystallization isotherm of LDPE/LDPE-g-MAH/Ag-NPs (95.5:3:1.5): (1) 50, (2) 100, (3) 150 and (4) 200°C min^{-1} cooling rates in coordinates $[1/(1-X_t)](\mathrm{d}X_t/\mathrm{d}t)$ *vs.* X_t; solid line represents the result calculated by using the macrokinetic Malkin equation and symbols indicate the results calculated by using the Avrami equation.

Malkin equation in the coordinate axes $[1/(1-X_t)](\mathrm{d}X_t/\mathrm{d}t)$ *vs.* X_t at different cooling rates for virgin LDPE. The fitting of data points indicate that the experimental data are sufficient, except for the final region, where there is a higher degree of percentage of crystallinity. A similar trend in graphs is also observed in case of LDPE/LDPE-g-MAH/Ag-NPs (95.5:3:1.5) nanocomposite film (see figure 15). It is seen that the fit of the Avrami equation to experimental data is not good at the end stage of the crystallization process. This is the reason for the mismatch of the 'dots' and solid lines in figures 14 and 15, which may be regarded as an argument in favour of eq. (22).

In case of the Malkin approach, the author has adopted a shortcut method of calculating the crystallization kinetics parameters (C_0 and C_1) taking into consideration the Avrami approach. Primarily, C_0 relates directly to the Avrami exponent n_a according to the following relation [16]:

$$C_0 = 4^{n_a} - 4, \tag{25}$$

Table 6. Summary of Malkin parameters (C_0 and C_1).

Materials	λ (°C min^{-1})	C_0	C_1
Virgin LDPE	5	529.7425	0.833333
	10	429.5336	0.862069
	15	423.5651	1.020408
	20	248.4756	1.190476
LDPE/LDPE-g-MAH/ Ag-NPs (95.5:3:1.5)	5	851.1314	1.166861
	10	644.0674	2.227171
	15	441.7219	2.518892
	20	99.9683	2.577321

and C_1 relates to the Avrami kinetic parameters as follows [16]:

$$C_1 = \frac{(\ln(4)^{n_a} - 2)}{(\ln 2)^{1/n_a}} K_a. \tag{26}$$

Without using the data-fitting procedure to determine C_0 and C_1, these parameters can be estimated from eqs (5) and (6). Table 6 summarizes the Malkin kinetics parameters.

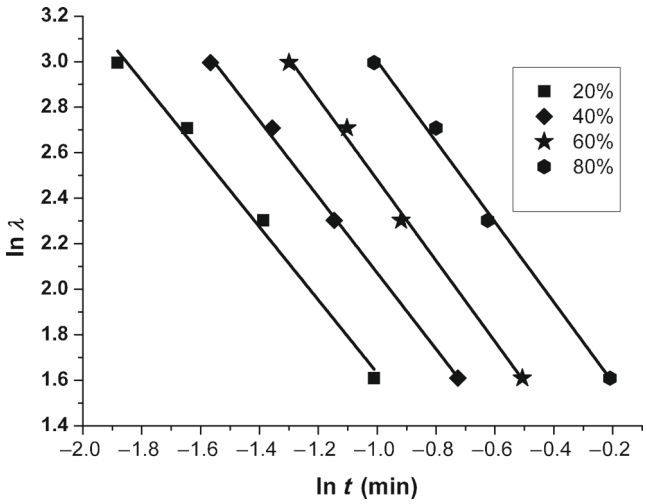

Figure 16. Mo plots of $\ln\lambda$ as a function of $\ln(t)$ for crystallization of virgin LDPE at different percentages of relative crystallinity.

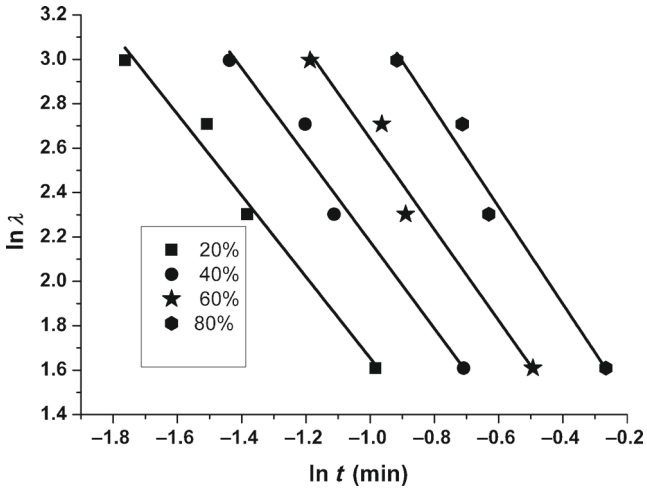

Figure 17. Mo plots of $\ln\lambda$ as a function of $\ln(t)$ for crystallization of LDPE/LDPE-g-MAH/Ag-NPs (95.5:3:1.5) nanocomposite film at different percentages of relative crystallinity.

Table 7. Kinetics parameters at different relative degrees of crystallinity using the Mo equation.

Materials	X_t (%)	α	$\ln F(T)$	$F(T)$
Virgin LDPE	20	1.611	0.71609	2.03
	40	1.680	1.08887	2.96
	60	1.761	1.39667	4.01
	80	1.784	1.93221	6.88
LDPE/LDPE-g-MAH/ Ag-NPs (95.5:3:1.5)	20	1.826	0.52596	1.68
	40	1.948	0.92256	2.51
	60	2.042	1.29172	3.63
	80	2.180	1.72021	5.58

The Malkin exponent C_0 is found to be in the range of 99.96–529.74.

5.2b3 *Comparison of modelling results*: As discussed, the kinetic parameters obtained using the Malkin macrokinetics model are found to be high as compared with those of the Avrami model. This might be due to Malkin's equation, which is derived from the differential macrokinetic concept. The differences in kinetic parameters were not understood due to experimental error.

A method was proposed by Mo and co-workers to describe the non-isothermal crystallization kinetics. The Mo equation is

$$\ln\lambda = \ln F(T) - \alpha \ln(t), \tag{27}$$

where $F(T)$ refers to the cooling rate at unit crystallization time and α is the ratio of the kinetic parameter (exponent) of Avrami to Ozawa exponent.

Figures 16 and 17 show plots of $\ln\lambda$ *vs.* $\ln(t)$ for virgin LDPE and LDPE/PE-g-MAH/Ag-NPs (95.5:3:1.5) nanocomposite film. From the plots a linear correlation between $\ln\lambda$ and $\ln(t)$ has been derived. By the linear fitting method, the slope $(-\alpha)$ and the intercept $[\ln F(T)]$ have been calculated and listed in table 7. The values of α for virgin LDPE vary from 1.61 to 1.78 and for LDPE/LDPE-g-MAH-Ag-NPs (95.5:3:1.5) nanocomposite film they vary from 1.82 to 2.18. The value of α is nearly the same for each of the sample. The values of $F(T)$ increase steadily with the increase in relative degree of crystallinity, indicating that a higher cooling rate should be required in order to obtain a higher degree of crystallinity. The values of $F(T)$ for virgin LDPE are greater than that for LDPE/LDPE-g-MAH/Ag-NPs (95.5:3:1.5) nanocomposite film, which implies that the necessary cooling rate for virgin LDPE is larger than that of nanocomposite film. Since $F(T)$ reflects the complexity of the crystallization process, the smaller values as obtained for the Ag-NPs loaded nanocomposite film at the respective cooling rate reflects faster rate of crystallization.

6. Morphological analysis

6.1 *XRD analysis*

XRD spectroscopy can be used to estimate the degree of dispersion of Ag-NPs in the PE matrix. XRD data of Ag-NPs and PE/PE-g-MAH/Ag-NPs (95.5:3:1.5) nanocomposite film are shown in table 8. The diffraction peaks at 38.1, 44.3, 64.5 and 77.4° represent, respectively, the crystallographic planes of (111), (200), (220) and (311) for the face-centered cubic (FCC) structure of the silver crystal as shown in figure 18.

Ag-NPs have a different crystal size, which has been calculated using the Scherrer equation (eq. (28)) and listed in table 8:

$$t = (KX\lambda)/B\cos\theta_b, \tag{28}$$

Table 8. Peak properties of Ag-NPs and LDPE/LDPE-g-MAH/Ag-NPs nanocomposite film.

Peak position of Ag-NPs	Peak properties	Ag-NPs	LDPE/LDPE-g-MAH/Ag-NPs (95.5:3:1.5) nanocomposite film
111	Peak position 2θ	38.06	38.27
	Peak width $\beta_{1/2}$	0.2598	0.3936
	D-spacing	2.598	2.3517
	Crystal size	33.81	22.33
200	Peak position 2θ	44.45	43.486
	Peak width $\beta_{1/2}$	0.1948	0.393
	D-spacing	2.037	2.0675
	Crystal size	46.05	22.74
220	Peak position 2θ	64.13	64.468
	Peak width $\beta_{1/2}$	0.4546	0.944
	D-spacing	1.452	1.442
	Crystal size	21.56	20.4
311	Peak position 2θ	77.408	
	Peak width $\beta_{1/2}$	0.6336	
	D-spacing	1.2319	
	Crystal size	16.79	

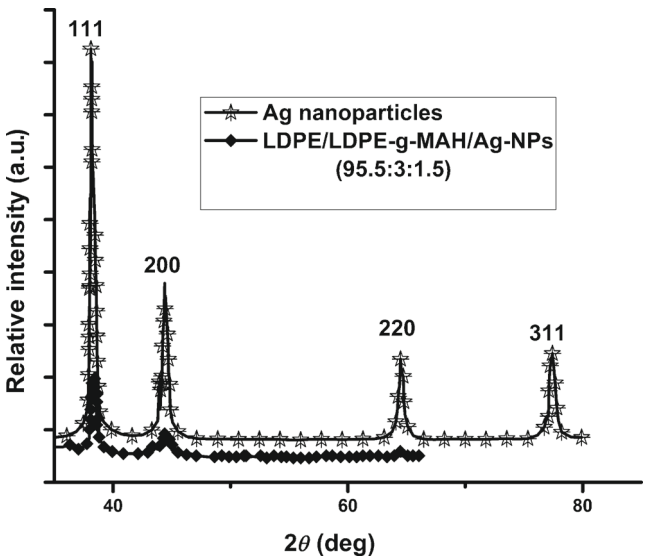

Figure 18. XRD plots of Ag-NPs and the LDPE/LDPE-g-MAH/Ag-NPs (95.5:3:1.5) nanocomposite film.

where t is crystallite thickness in nm, K is a constant (0.91–1 for Ag-NPs), λ is X-ray wavelength (1.54 Å), B is full width at half maximum (FWHM) of the peak at $d_{001} = 2\Delta\theta$ and θ_b is diffraction angle at FWHM (in radian).

The LDPE/LDPE-g-MAH/Ag-NPs (95.5:3:1.5) nanocomposite film shows diffraction peaks at 38.27, 43.48 and 64.46°, which are slightly lower in angle than those of Ag-NPs diffraction peaks at the same peak position (figure 18). The marginal decrease in the crystallite size in the compatibilized nanocomposite film can be ascribed to the possible dispersal of Ag-NPs in the PE matrix. In principle the crystallite size of Ag-NPs can be determined using WAXD but this is rarely the case in practice. It is because at any given point in time, there will be a wide range of crystallite sizes.

6.2 *Transmission electron microscopy (TEM)*

TEM micrography is a method to visualize the dispersion of nano-filler with the polymer matrix. In order to compare the morphological investigation result as obtained from XRD analysis, high-resolution TEM micrographs of melt-blended LDPE/LDPE-g-MAH/Ag-NPs (95.5:3:1.5) nanocomposite film have been analysed. Figure 19 shows high-resolution TEM micrographs of the LDPE/LDPE-g-MAH/Ag-NPs (95.5:3:1.5) nanocomposite film. It is seen that Ag-NPs are well distributed in the polymer matrix, suggesting strong interaction of Ag-NPs with the polymer matrix. It has been observed that a small fraction of Ag-NPs form agglomeration and they are found at different places in the micrographs. In spite of the small amount of aggregation formed in the nanocomposite film, improvement in overall properties of the nanocomposite film was observed [40,41].

7. Conclusions

LDPE/LDPE-g-MAH/Ag-NPs (95.5:3:1.5) nanocomposite films were prepared employing the melt intercalation technique. The effect of Ag-NPs on mechanical, thermal and morphological properties has been investigated. The tensile modulus of LDPE/LDPE-g-MAH/Ag-NPs (95.5:3:1.5) nanocomposite films was less as compared with the virgin matrix for Ag-NPs 0.5 and 2.5 wt% loading. On the other hand 1.5-wt%-loaded nanocomposite film shows increased modulus value as compared with virgin LDPE. The addition of compatibilizer has little effect on the mechanical

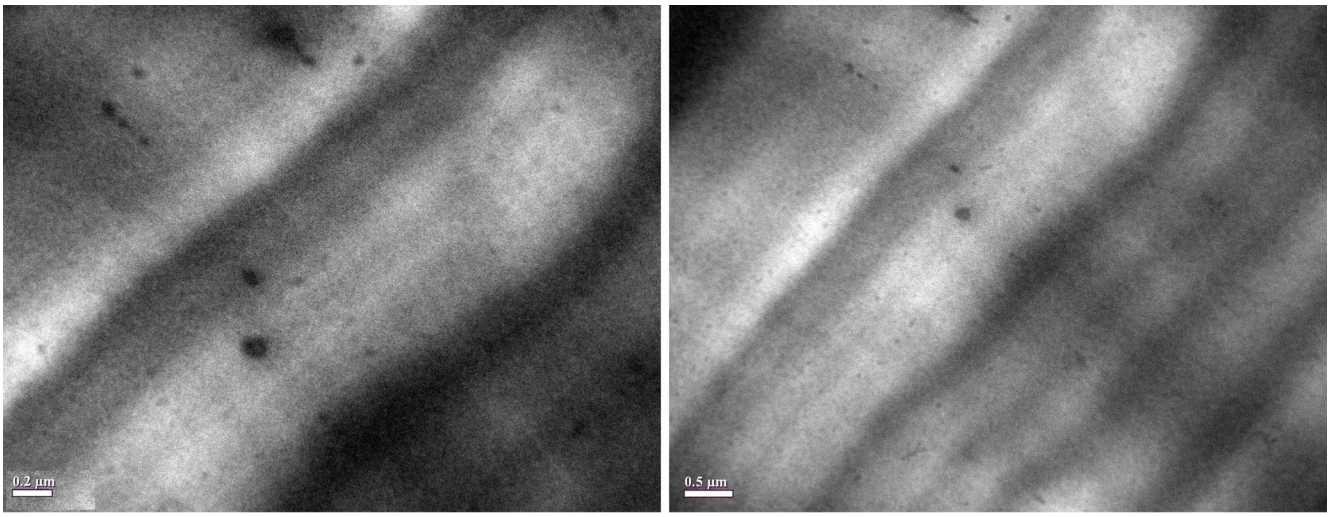

(a) (b)

Figure 19. Representative high-resolution TEM images of LDPE/LDPE-g-MAH/Ag-NPs (95.5:3:1.5) nanocomposite films.

properties of the nanocomposites. As compared with virgin LDPE, the nanocomposite exhibited an improved thermal stability. From thermal analysis, it is seen that on addition of Ag-NPs as reinforcing agent into the LDPE matrix, crystallization temperature was increased by 3°C. Further, $t_{1/2}$ required for the crystallization decreases up to 16%, which confirms the heterogeneous nucleating behaviour of Ag-NPs. Non-isothermal crystallization kinetics of virgin LDPE and LDPE/PE-g-MAH/Ag-NPs (95.5:3:1.5) nanocomposite film revealed an increase in crystallization rate with the addition of Ag-NPs. Different macrokinetic models such as Avrami, Malkin and Mo models have been used to analyse the non-isothermal crystallization behaviour of the virgin polymer and its nanocomposites. It is revealed that the kinetics of crystallization of the LDPE matrix and its nanocomposite follows Avrami theory as well as Malkin theory. The nucleation proceeds by three-dimensional spherulite growth with simultaneous homogeneous and heterogeneous nucleation. The macrokinetic modelling is supplemented by detailed discussion of the relevant kinetic parameters and their dependence upon cooling rates. The exponent n_a, in the range of 3–5, indicated a very intricate crystallization mechanism in these samples. The value of K_a was found to be higher for LDPE/PE-g-MAH/Ag-NPs (95.5:3:1.5) nanocomposite film than that of virgin LDPE, which shows the larger rate of crystallization in case of nanocomposite than that for virgin polymer. From the Mo method of crystallization study it is revealed that the value of $F(T)$ was lower for the LDPE/PE-g-MAH/Ag-NPs (95.5:3:1.5) nanocomposite film than that of virgin LDPE, demonstrating the higher rate of crystallization in the presence of Ag-NP-loaded LDPE matrix, which is in agreement with Avrami analysis results. The good adhesion between Ag-NPs and LDPE matrix was confirmed from the high-resolution TEM images of the compatibilized-nanocomposite film. Some agglomeration of Ag-NPs was also observed from the high-resolution TEM images. Therefore, Ag-NPs not only acted as a nucleating agent for virgin LDPE but also limited the chain mobility. Hence, the competition between the two conflicting roles of the Ag-NPs determines the overall crystallization kinetics behaviour of nanocomposite film.

Acknowledgement

This research received no specific grant from any funding agency in the public, commercial or not-for-profit sectors.

References

[1] Bastarrachea L, Dhawan S and Sablani S S 2011 *Food Eng. Rev.* **3** 79
[2] Jokar M, Rahman R A, Ibrahim N A, Abdullah L C and Tan C P 2012 *Food Bioprocess Technol.* **5** 719
[3] Hsu C C, Geil P H, Miyaji H and Asai K 1986 *J. Polym. Sci. Part B:Polym. Phys.* **24** 2379
[4] Zhang X M, Elkoun S, Ajji A and Huneault M A 2004 *Polymer* **45** 217
[5] Kaiser E J, Mcgrath J J and Bénard A 2000 *J. Appl. Polym. Sci.* **76** 1516
[6] Liu T, Mo Z, Wang S and Zhang H 1997 *Polym. Eng. Sci.* **37** 568
[7] Avalos F, Lopez-Manchado M A and Arroyo M 1996 *Polymer* **37** 5681
[8] Avrami M 1939 *J. Chem. Phys.* **7** 1103
[9] Avrami M 1939 *J. Chem. Phys.* **8** 212
[10] Avrami M 1939 *J. Chem. Phys.* **9** 177
[11] Ozawa T 1971 *Polymer* **12** 150
[12] Tobin M C 1974 *J. Polym. Sci.:Polym. Phys.* **12** 399
[13] Tobin M C 1974 *J. Polym. Sci.:Polym. Phys.* **14** 2253
[14] Tobin M C 1974 *J. Polym. Sci.:Polym. Phys.* **15** 2269
[15] Malkin A Y, Beghishev V P and Keapin I A 1983 *Polymer* **24** 81

[16] Malkin A Y, Beghishev V P, Keapin I A and Bolgov S A 1984 *J. Polym. Eng. Sci.* **24** 1396

[17] Mubarak Y, Harkin-Jones E M A, Martin P J and Ahmad M 2001 *Polymer* **42** 3171

[18] Supaphol P 2001 *Thermochim. Acta* **370** 37

[19] Zhang Z, Xiao C and Dong Z 2007 *Thermochim. Acta* **466** 22

[20] Wu H, Liang M and Lu C 2012 *Thermochim. Acta* **545** 148

[21] Wang S and Zhang J 2014 *J. Therm. Anal. Calorim.* **115** 63

[22] Malkin A Y, Beghishev V P and Bolgov S A 1982 *Polymer* **23** 385

[23] Zhishen M O 2008 *Acta Polym. Sin.* **7** 656

[24] Zhang Z 1993 *Chin. J. Polym. Sci.* **11** 125

[25] Johnson W A and Mehl K F 1939 *Trans. Am. Inst. Mining Met. Eng.* **135** 416

[26] Supaphol P and Spruiell J E 2001 *Polymer* **42** 699

[27] Wunderlich B 1976 *Macromolecular physics* (New York: Academic Press)

[28] Pérez-Ćardenas F C, Castillo L and Vera-Graziano R 1991 *J. Appl. Polym. Sci.* **43** 779

[29] Malkin A Y, Bolgov S A, Begishev V P and Mazalov O S 1991 *J. Eng. Phys.* **61** 1092

[30] Mandelkern L 1964 *Crystallization of polymers* (New York: McGraw Hill)

[31] Azlin-Hasim S, Cruz-Romero M C, Morris M A, Cummins E and Kerry J P 2015 *Food Pack. Shelf Life* **4** 26

[32] Pongnop W, Sombatsompop K, Kositchaiyong A and Sombatsompop N 2011 *J. Appl. Poly. Sci.* **122** 3456

[33] Hanemann T and Szabó D V 2010 *Materials* **3** 3468

[34] Tjong S C and Bao S 2007 e-Polymers **7** 1618

[35] Pant B, Pant H R, Pandeya D R, Panthi G, Nam K T, Hong S T and Kim H Y 2012 *Colloids Surf. A:Physicochem. Eng. Aspects* **395** 94

[36] Lee J M, Kim D W, Jun Y D and Oh S G 2006 *Mater. Res. Bull.* **41** 1407

[37] Kamal M R and Chu E 1983 *Polym. Eng. Sci.* **23** 27

[38] Abareshi M, Zebarjad S M and Goharshadi E K 2014 *Bull. Mater. Sci.* **37** 1113

[39] Zhu X L, Wang C S, Wang B and Wang H P 2008 *Iran Polym. J.* **17** 297

[40] Salah H B H, Daly H B, Perrin F and Denault J 2011 *Sci. Eng. Compos. Mater.* **18** 173

[41] Zapata P A, Tamayo L, Páez M, Cerda E, Azócar I and Rabagliati F M 2011 *Eur. Polym. J.* **47** 1541